Background reduction at DTU Nutech surface gamma laboratory

Marković, Nikola; Roos, Per; Nielsen, Sven Poul; Cai, Xiao Xiao

Published in:
Applied Radiation and Isotopes

Link to article, DOI:
10.1016/j.apradiso.2019.05.014

Publication date:
2019

Document Version
Peer reviewed version

Background reduction at DTU Nutech surface gamma laboratory

Nikola Marković[1], Per Roos, Sven Poul Nielsen, Xiao Xiao Cai
Technical University of Denmark
Center for Nuclear Technologies, Frederiksborgvej 399, 4000 Roskilde, Denmark

Abstract
Sources of background and background variation in a BEGe type HPGe detector located in a surface laboratory were identified. Different strategies for background reduction were applied.
A cosmic veto was installed, and optimised using a digital acquisition system in list-mode with time-stamped data. This resulted in the reduction of total background by a factor of 1.4. Thermal and fast neutron fluxes were also calculated. The radon induced background component and its variation were significantly reduced.

Keywords: cosmic veto, HPGe detector, low-level, anticoincidence, gamma spectrometry.

1. Introduction

Gamma-ray spectrometry using high-purity germanium (HPGe) detectors is the most prevalent (radiometric) method for determination of radionuclides. Its applications range from measurements of very high activities in radiopharmaceuticals, to low activity levels in environmental samples, and extremely low levels encountered in rare events detection. When low activity levels are measured low background detectors are used, with samples placed close to the detector and measured over extended periods of time. In some cases (Agostini et al., 2013), even the detector material itself can become a "sample". Systems can be roughly divided to low-level and ultra low-level depending upon the activity levels that can be reached. For low-level applications special radiopure materials are used for shielding and in detector production. Additional measures for background reduction must be undertaken for ultra low-level; these can include placing the detectors in underground laboratories (Hult, 2007).

It is clear that background is an important factor in gamma-ray spectrometry. Usually, background spectra are obtained when there is no sample present in a detector. Another possibility involves the measurement of an empty beaker without the sample in, but that is rarely practiced. As with any normal spectrum, background comprises both peaked background and continuous background (from Compton, bremsstrahlung or charged particle interactions in detector). Counts in peak are important because they need to be subtracted from the counts measured with a sample on. Continuous background counts do not affect measurements directly, but together with the continuum coming from the sample itself (and the counts in peak if present) they determine the performance of the system through detection limits. According to (Currie, 1968) detection limit is proportional to the square root of background in the region of interest for a specific gamma line; therefore, the influence of background is more important for activity calculation where the contribution is linear (peaked background). When calculating detection limits the metrology community refers generally to the ISO 11929 approach (IAEA, 2017; ISO, 2019).

Good knowledge and control over background in gamma spectrometry is crucial not only to improve detection limits but also for reducing variability in background affecting measurement results (Dragounová and Rulík, 2013; Hult et al., 2013; IAEA, 2017; Yoho et al., 2016); this is often

[1] Present address: Department of Radiation Physics, Institute of Clinical Sciences, Sahlgrenska Academy, University of Gothenburg, Gothenburg, Sweden, nikola.markovic@gu.se

neglected. Background contribution (total and variability) becomes even more significant for lower activity measurements, therefore in low-level laboratories background is particularly important parameter.

Many factors may lead to changes in background. Detector or in-shield contamination by a sample, or small changes in shield geometry (usually in moving parts, such as the closing system etc.) will induce a sharp change. Airborne radon concentration in the laboratory can be significant, and is affected by seasonal variations and meteorological conditions (Maver Modec et al., 2012) but the most important is stability of laboratory ventilation. Deposition of radon and progenies onto plastic beaker surfaces due to static charge has been observed (Heusser, 1991; Turunen et al., 2011). Care should be taken with detector plastic covers used for protection (from contamination or window damage). It is recommended that all measurements start with a delay (after placing the sample and closing the shield) to allow for a decay of short-lived ^{222}Rn daughters. Improper radon background management can have high impact on ^{226}Ra activity determination over ^{214}Bi and ^{214}Pb daughters (Mauring et al., 2014). Changes in cosmic radiation flux can also introduce background variability.

In combination, these factors can significantly affect measurement results. For standard gamma spectrometric applications this can result in the reporting wrong activity values or decision limits; sometimes the unexpected results may even be misinterpreted and mistakenly explained as decay law violation (Pommé et al., 2016). If counting uncertainty is used solely as the uncertainty for background peaks this will underestimate the total uncertainty in the background because of variability (Lépy et al., 2015). That is why background spectra should be recorded routinely in order to account for variability and to detect possible sharp changes in the background. Ideally, this should be coupled with a good quality assurance system in order to fully take background variability into account, as in (Bruggeman et al., 2014).

In this work, we present an analysis of background components in a typical low-level surface gamma laboratory used for the routine measurement of environmental and radioecological samples. Contributions from different background sources are estimated and different background remediation strategies tested: active cosmic veto detection for the reduction of the cosmic background component, and flushing with the boil-off gas of the nitrogen dewar for the reduction of airborne radon concentration inside the shield. Reducing the cosmic ray background component enables reaching lower detection limits, but by reducing general background continuum it also enhances the counting statistics in environmental background peaks (e.g. radon progeny) thus enabling more effective monitoring of background variability (Hult et al., 2012).

2. Experimental setup

The Radioecology section of DTU Nutech operates 18 HPGe detectors with relative efficiencies ranging from 15% to 50%. Of those, 15 are used for routine measurements, where samples are changed and spectra evaluated by technicians. For quality control, sources of evaporated ^{241}Am, ^{137}Cs and ^{60}Co embedded in epoxy glue in glass LSC vials are measured monthly to check the efficiency and energy calibration of the detectors. Short background checks are often performed, while long background measurements are taken once or twice per year (usually over holidays). Gamma laboratories are situated in a single storey building with no overburden (there is no concrete slab/plate above, only a thin roof). In this kind of circumstance, the cosmic induced background will be much higher than in similar laboratories situated under several storeys of a building. This however is considered inconsequential, as low-level gamma spectrometry is not the main strength of the DTU Nutech Radioecology section; the expertise is in radiochemistry, which is used for concentrating the radionuclides of interest in low activity samples.

This work will focus upon one of the three Canberra broad energy range, BEGe 5030, type detectors procured in 2016 (late 2015), named detector 8 (DET08). The detectors are intended for routine use

and provide good resolution and optimal efficiency for the wide range of samples measured (mostly activity in food and the environment). The detectors are placed in 10 cm thick shields (Fig. 1), manufactured in the years 70's and 80's from lead with a low ^{210}Pb content (mainly supplied from Boliden and Goslar). Radon contribution to the background is proportional to the radon concentration in laboratory air and the volume of free space surrounding the detector inside the lead shield (Theodórsson, 1996). The shields have a large free volume and are not tight with the expectation that the resulting radon background will be significant. Shields have different inner linings for Pb X-ray fluorescence attenuation. Detector 8 is equipped with 1 mm cadmium inner lining. Detector 8 has ~50% relative efficiency (germanium crystal diameter 81 mm, thickness 31 mm) with an ultra-low background dipstick cryostat (Model 7500SL-RDC-6-ULB) and a remote preamplifier. The detector has 0.6 mm thick carbon epoxy window. One plastic (polyvinyltoulene) sheet manufactured by Scionix (model R400x50B500) with 5 cm active thickness was used as an active cosmic veto detector. The veto was placed outside on the top of lead shield (Fig. 1). Acquisition for routine measurements was done using a standard amplifier – Canberra multiport chain. Digital list-mode acquisition was used with a veto. A CAEN DT5781P digital multichannel analyser was utilized for list-mode acquisition, enabling time-stamped data collection with a 10 ns time resolution and 15-bit ADC resolution. Genie 2000 spectra were generated using MATLAB based coincidence analysis software, as described in (Marković et al., 2018, 2017a). For the peak location and area calculation Canberra Genie 2000 software (Canberra, 2013) was used via the interactive peak fit package (Canberra, 2009).

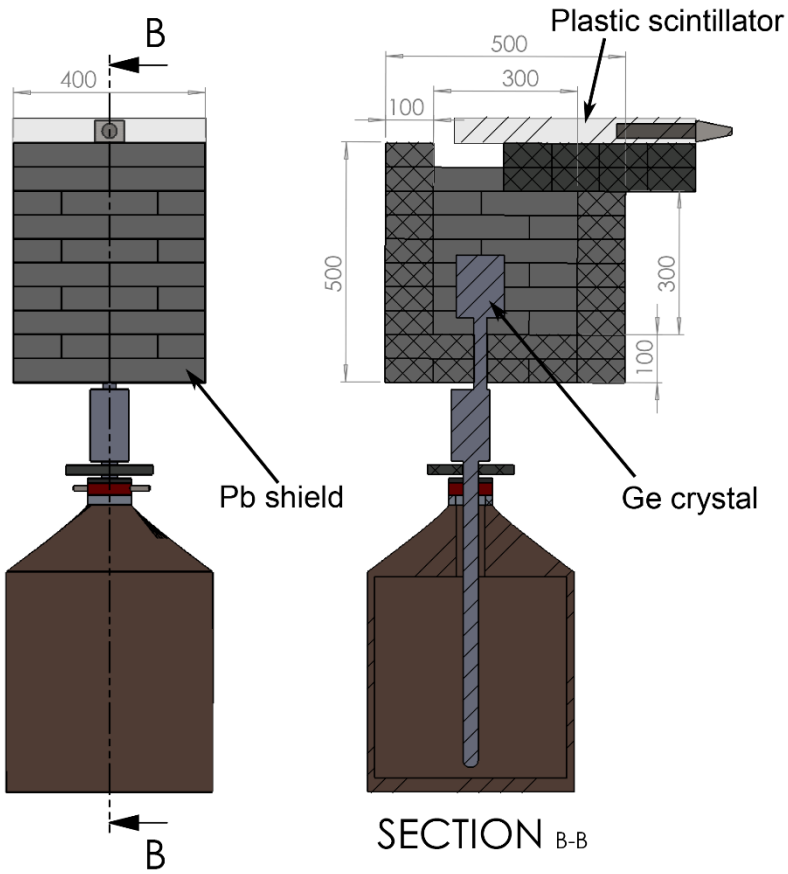

Fig. 1 Schematic representation of a BEGe detector inside a lead shield with a plastic veto plate placed on top (dimensions in mm). The shield opens by sliding the lid.

3. Results

3.1. Background variability and radon contribution

The background on detector 8 was measured regularly over two years. Fig. 2 (b and c) shows the background variation in ten measurements taken between March 2016 and October 2017. Measurement times range from 2 to 10 days with an average of 5 days. Relative variation in the integral count rate is less than 5%, while the count rates in peaks originating in cosmic activation of detector and shielding material vary less than 20%. No lines overlapping with neutron activation lines are selected in our nuclide library; therefore, any variations in that part of background contribute to the measurement results only via Minimum Detectable Activity (MDA) determination where they come in as a square root of background counts. Consequently, the effect of variation should not be important. Sporadic excess in thermal neutron flux from the medical cyclotron in a nearby laboratory has been observed. Although situated around 100 m away, when operating in specific mode and with reduced shielding, its influence can be seen in the spectra as increase in count rate of Cd neutron activation lines.

Variation in radon daughter count rates is clearly important, (Fig. 2 a). If only the counting uncertainty of a single background measurement is considered for the total uncertainty of a selected background line, this will significantly underestimate the total uncertainty dominated by background variability[2]. Table 1 shows average, minimum and maximum count rates in the three most pronounced lines originating from radon progeny and the ^{40}K line. Variation in radon daughter count rates rises up to a factor ~3, while variation in the ^{40}K peak count rate is less than 20%. Radon progeny variation is a consequence of the varying radon concentration in lab air, while ^{40}K may arise from small differences in shield geometry (for example, incomplete lid closing) or LN2 filling (LN2 shielding effect has not been examined). When the effect of background variability on ^{214}Bi and ^{214}Pb determination is evaluated, a bias of up to 0.3 Bq per sample (or 20 Bq/kg depending on sample size) is calculated. This is the bias that can be introduced to activity calculation if background variability is neglected, Table 2. After the introduction of boil-off nitrogen gas, these were reduced for more than an order of magnitude.

The effect on ^{40}K determination is less but still significant because of the lower full energy peak (FEP) efficiency for 1.5 MeV photons, and the lower gamma emission probability for ^{40}K. Here we neglected the effect of sample shielding in the detector (by reducing the available volume inside the shield and by attenuation of gamma rays) that would reduce radon background component with the sample on. Shielding factors should be estimated either by measurements of blank samples or by modelling (Korun et al., 2014). Daily (diurnal) radon oscillations although prominent (Mauring et al., 2014) are also neglected. They do not make a significant impact on low activity measurements as low activities are measured over a few days, resulting in the high frequency background oscillation being averaged (Maver Modec et al., 2012).

Fig. 3 shows the dependence of integral background count rate in the 40-2100 keV region on the sum of count rates in the 295 keV, 352 keV and 609 keV peaks. The two count rates are strongly correlated with Pearson's linear correlation coefficient of 0.97 ($p<0.0001$). If extrapolated to zero, the ^{222}Rn background contributes 1.24 cps to the total background count rate. Taking into account an average background count rate of 1.27(0.03) cps we calculate the average radon contribution to be less than 3% of the total background.

The radon background component, although insignificant in the total background, has a strong impact on ^{222}Rn progeny determination. Therefore, we decided to reduce that background component. First, by covering the shield with a simple motor boat cover (Sea Cover 420D 75x75x45 cm 420D

[2] Proper estimates for the net background count rate and its uncertainty for variable background are given in (IAEA, 2017), Section 5.4.5.7.

polyester), it was possible to reduce air exchange between the lab and inside of the shield. Then nitrogen boiling off the Dewar was fed through a small hole inside the shield, in order to create overpressure, and further reduce air coming inside the shield. A special plug was manufactured tightly closing the nitrogen filling inlet; a hose was mounted on the outgassing port and fed into the shield. The third outlet (safety) was not blocked. A significant reduction in the amount of variation in the radon component (Table 1) was observed, but in order to confirm the stability further measurements are needed. A reduction of the ^{40}K component was achieved by the re-alignment of some lead bricks and the introduction of a Pb ring between the preamplifier and a Dewar (Fig. 1). This was undertaken to further enhance the effect of the offset between the upper and lower part of the cryostat that shields the detector element from the vacuum sieves (Verplancke, 1992). No lead plate was present under the Dewar so the inclusion of a lead ring in this position blocks a direct line of sight from the ground to the crystal, absorbing a part of ^{40}K photons. The flow-rate of boil-off nitrogen was calculated to be between 0.6 and 1 l/min. A test was made by using nitrogen from a pressurized cylinder (that had been left for 2 months to allow any possible radon contamination to decay), and flow-rates ranging from 0.6-4 l/min, but no significant changes have been observed. There was even a slight increase in the low energy count rate for 4 l/min flow. It could be due to the increased noise and vibration induced by such a high flow-rate. One remaining issue of concern is air exchange resulting from opening of the shield for sample changing. Our shields have a large free volume inside, therefore it is theoretically possible to introduce a lot of airborne radon in this way. The next step would be reducing the shield inner volume by introducing an ultra-pure lead plates. Until then, a ~4 hours delay between sample exchange (coupled with a fast exchange to minimise the time shield is open) and the start of the measurement will be introduced for low level measurements. That should be sufficient for ^{222}Rn progeny to decay, and possibly to exchange part of ^{222}Rn with venting nitrogen. In combination with the purging we expect background to be lower and more stable. Additional background measurements over longer period are needed to update new uncertainties for the optimized system.

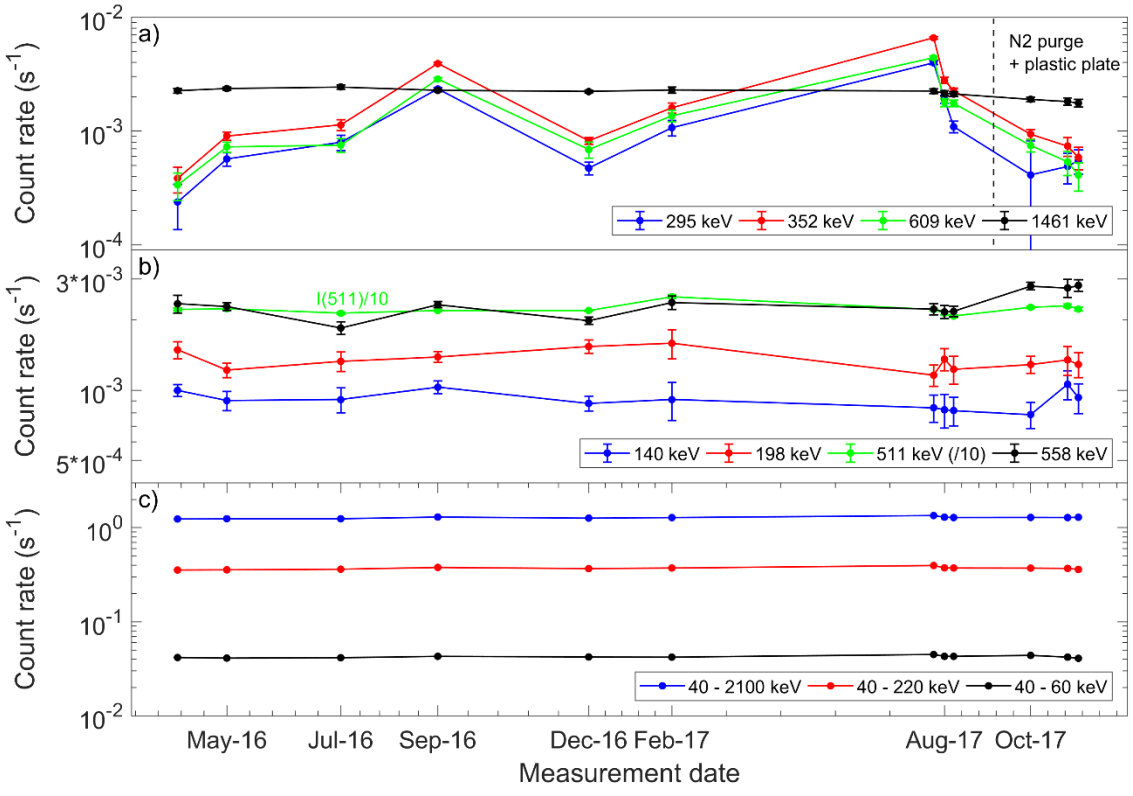

Fig. 2 Variation in background count rate of natural sources, radon daughters and ^{40}K, is shown in a). In September 2017, flushing with the boil-off gas from the nitrogen dewar was initiated, reducing the overall Rn background and its variability (indicated with vertical line). Variation in peak count rates of cosmic induced lines and integral background are shown in b) and c).

Table 1 Variation in background count rates before and after Rn reduction. Rn average values are reduced by a factor of 2-3 and variability up to an order of magnitude.

		Count rate before (s^{-1})			Count rate after (s^{-1})		
Source	E (keV)	Average	Max	Min	Average	Max	Min
^{214}Pb	295.22	1.3E-03	4.0E-03	2.4E-04	4.8E-04	5.5E-04	4.1E-04
^{214}Pb	351.93	2.1E-03	6.6E-03	3.8E-04	7.6E-04	9.4E-04	5.9E-04
^{214}Bi	609.31	1.5E-03	4.4E-03	3.4E-04	5.6E-04	7.5E-04	4.1E-04
^{40}K	1460.82	2.3E-03	2.4E-03	2.1E-03	1.8E-03	1.9E-03	1.8E-03

Table 2 Background variation effect on activity calculation for two standard beakers (before the radon component remediation was installed).

			Petri beaker (5 cm3, water)				Big beaker (300 cm3, water)			
			LabSOCS		Bias		LabSOCS		Bias	
	E (keV)	I_γ	ε_{FEP}	TCS	Bq/sample	Bq/kg	ε_{FEP}	TCS	Bq/sample	Bq/kg
^{214}Pb	295.2	18.414	1.3E-01	1.01	1.1E-01	2.2E+01	4.3E-02	1.00	3.3E-01	1.1E00
^{214}Pb	351.9	35.6	1.1E-01	1.00	1.1E-01	2.3E+01	3.7E-02	1.00	3.4E-01	1.1E00
^{214}Bi	609.3	45.49	6.5E-02	0.82	1.2E-01	2.4E+01	2.3E-02	0.89	3.1E-01	1.0E00
^{40}K	1460.8	10.55	3.0E-02	1.00	5.8E-02	1.2E+01	1.1E-02	1.00	1.6E-01	5.2E-01

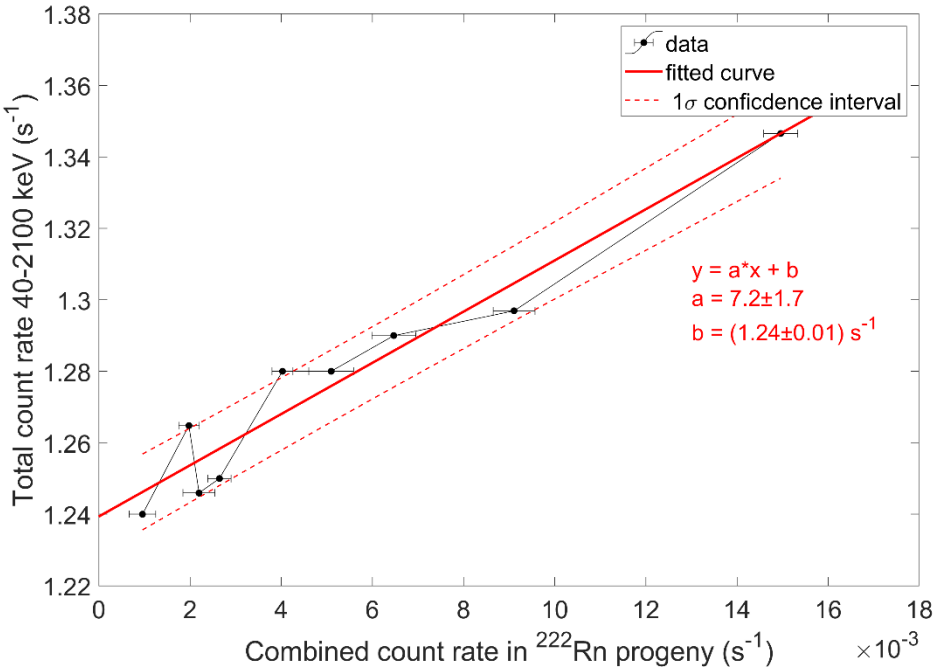

Fig. 3 Total spectrum count rate in the 40-2100 keV interval as a function of the sum of count rates in three radon daughter peaks (295 keV, 352 keV and 609 keV).

3.2 Muon component reduction

Muons are the most numerous charged particles at sea level, with relative intensities ($\mu^{\pm}$:n:$e^{\pm}$:p:$\pi^{\pm}$) 1420:480:340:13:1 (C. Patrignani et al. (Particle Data Group), 2016). Mean muon energy at ground level is ~4 GeV. Ionization processes and production of positrons dominate muon energy loss around this energy.

Active cosmic shield, or muon veto, is a special detector providing anticoincidence signal for the main HPGe detector. This way, events originating from muons depositing energy in both detectors are not counted by the main detector. It has been demonstrated that various types of detectors can be used for veto, e.g. (Agostini et al., 2015; Heusser, 1991; Rios et al., 2011), but plastic scintillators are considered the standard for gamma spectrometry applications (Burnett and Davies, 2014; Mrđa et al., 2007). Usually, the veto is placed outside the lead shield, and covers the shield from all sides (alternatively just the top surface if only one plate is available). In some special configurations, an in-shield veto can be added to enhance the muon shielding by detecting the muons that did not interact with the main shield (Heusser et al., 2015). This should not to be confused with a Compton veto. Environmental gamma background is also detected by the muon veto so the proper energy threshold should be selected in order to discriminate the environmental from the muon component and prevent unnecessary dead-time introduction. Veto detectors are usually designed so the environmental and muon component peaks are far enough apart to enable the setting-up of a proper lower level discriminator (LLD) to filter out the environmental gamma events. An additional lead shield around the veto can be used to shield against the environmental γ radiation (Gilmore, 2008; Heusser, 1995). Use of two veto plates operated in coincidence (Wieslander et al., 2009) is also possible. This method allows the long energy tailing of environmental gamma (from coincidence summing) to be rejected thus reducing the dead time. However, the use of coincidence criteria also reduces the efficiency for muon detection by counting only those events interacting with both plates (although not significantly; (Gastrich et al., 2016).

A plastic scintillator veto was placed over detector 8 and spectra from both detectors were saved in a list-mode with a time stamp for each detected event. On-board triggering in CAEN digital MCA was achieved with a RC-CR2 digital filter (CAEN Electronic Instrumentation, 2017); occurrence of the event (time stamp) corresponds to zero crossing of the RC-CR2 filter. In common with constant fraction discriminator triggering (CFD), it is independent of the pulse amplitude, but there may be some dependence on pulse rise-time (Leo, 1994). RC-CR2 signal was in this case smoothed using a moving average filter of 32 samples width. Fig. 4 shows the time distribution of coincidences between the HPGe and the veto detector (acquisition time is 5 days). Separation between the natural radioactivity γ rays and the energy deposited by muons was achieved using an energy threshold, as identified in Fig. 5. Coincidence time peak has an underlying structure resulting from the different processes that cause coincident detection (Fig. 4 insert). This can be explained by assuming that the coincidence spectrum in the HPGe detector has been generated for each delay range, Fig. 6. A sharp peak exists in a time spectrum at around 1.7 μs, arising from the interaction of muons in both detectors (from 0.8 to 2.2 μ). The delay is due to the different signal rise-times in the scintillator and the HPGe detector. The coincidence spectrum created with delays that cover the long tail of the coincidence time peak (3.4-15 μs, Fig. 6 blue spectrum) has a pronounced 13.2 keV peak, and an annihilation 511 keV peak. The low energy 13.2 keV peak is generated by de-excitation of the first level in ^{73}Ge with a 2.92 μs half-life (Singh, 2004). When stopped in the detector or surrounding material, the positively charged muons decay with a mean lifetime of about 2.2 μs, into two neutrinos and a positron. Positron annihilation generates a 511 keV peak in the spectrum. If the 3.4-15 μs part of the time spectrum in Fig. 4 is fitted to an exponential decay function, a 2.8 μs mean lifetime is calculated. This is a combination of a positive muon lifetime and slower activation product de-excitation.

In the spectrum generated with a 2.2 to 3.4 μs coincidence delay, a ^{72*}Ge broad neutron activation line is visible (~700 keV broad peak in the red spectrum Fig. 6). The delay results from negative muon decay that has the same lifetime as the positive muon in free space but decays faster when stopped in material due to muon capture (Zhang et al., 2017).
Peak broadening then occurs because of fast de-excitation (^{72*}Ge half-life = 400 ns; (Abriola and Sonzogni, 2010) compared to charge collection time, and leads to the collection of electron hole pairs generated by the recoil of the nucleus (taking a part of the neutron energy from inelastic scattering).

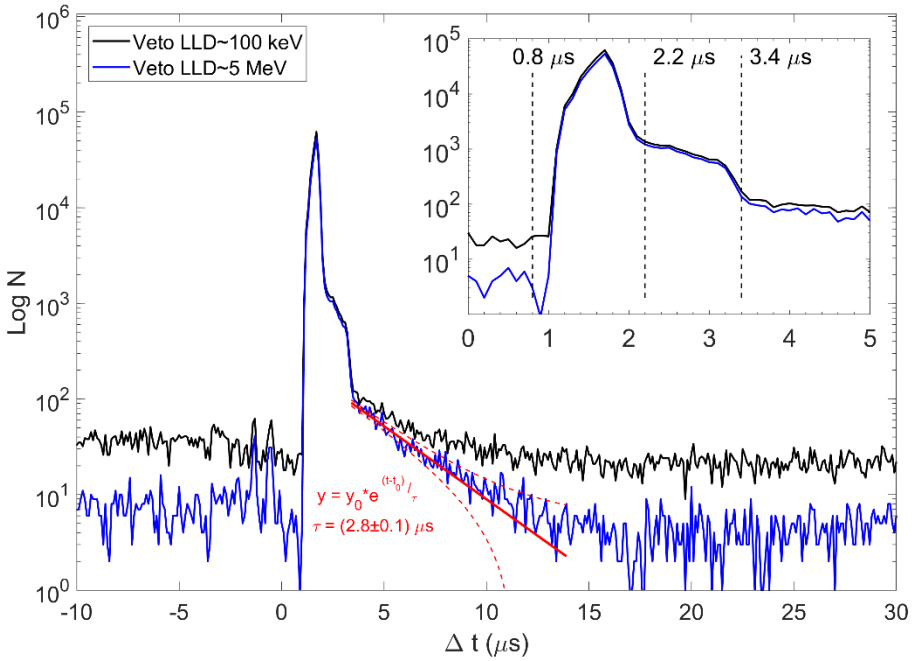

Fig. 4 Time distribution of differences in signal generation between the coincident events in the HPGe, and the veto detector (time when an event is registered in the HPGe, minus the time stamp of the closest veto event). If environmental background counts are not discriminated in the veto detector, then random coincidence continuum is high (black curve). By setting the LLD to around 5 MeV on the veto detector, the random coincidence count rate is reduced, and timing properties become clearer.

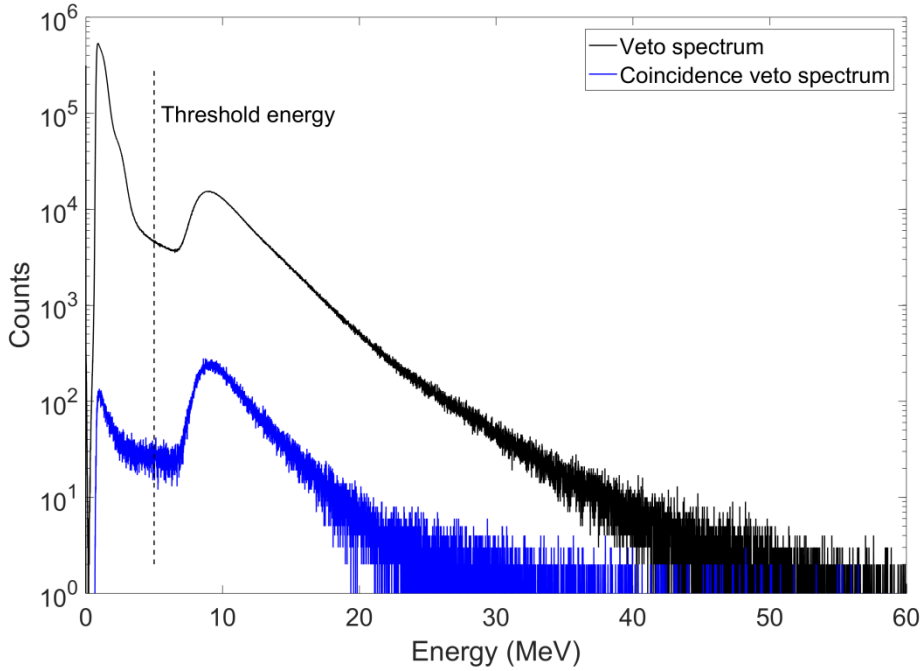

Fig. 5 Cosmic veto detector spectra generated over a 5 day interval. Spectrum of coincidences for the HPGE detector (15 μs width and 0.8 μs delay) is shown in blue. The peak centred around 10 MeV originates from muons passing through the plate. For the low energy range (up to 3 MeV), the source is environmental background radiation. Threshold energy for separation of environmental background and muon events is set in the middle of plateau between the two peaks, at around 5 MeV. It is used in conjunction with time coincidence to reduce random coincidences between the environmental background in the veto detector and counts in the HPGe detector.

Fig. 7 shows background spectra for a 15 day measuring period. Both spectra are generated from a single list-mode measurement with an ADC resolution of 16384 channels (0.18 keV per channel), but have been rebinned to 4096 channels (0.72 keV per channel) so the peaks are more apparent. Veto ON spectrum is obtained by selecting anticoincidence criterion with the veto detector, while the veto OFF is has been generated directly from the list file of the HPGe detector. The bottom part of the figure illustrates the reduction factor (per 4 bins), and is calculated as a ratio of the original spectrum and the anticoincidence spectrum: $I(\text{veto OFF})/I(\text{veto ON})$. The reduction factor shows a weak energy dependence rising from 1.25 at the lower energy region, up to 1.75 on the high-energy part of the spectrum, with an average of 1.45. Energy dependence occurs as a consequence of change in the relative contribution from the muon component to the total background. Natural background component falls with increasing energy (as does detector efficiency for gamma photon detection); at around 200 keV ^{210}Bi bremsstrahlung becomes significant, and at very low energies microphonic (and electronic) noise contributions start to appear. As expected, lines originating from natural background (^{40}K, ^{214}Bi, ^{214}Pb, ^{208}Tl) are seen as outliers, as the total peak areas are not changed. Neutron induced background lines (558.5 keV ^{114*}Cd, 803.1 ^{206*}Pb and Ge lines) also become less pronounced than overall continuum. The annihilation peak on the 511 keV and Cd X-ray lines are reduced, but remain above the average.

If this background reduction is accounted for in the calculations presented in (Marković et al., 2017b), a new ^{210}Pb MDA value of 75 mBq for a standard sediment sample, and a 5 day counting is obtained. This is a 14% improvement when compared to the reported value of 87 mBq. While not huge leap forward, it does deliver a 1.3 day shorter counting time to achieve the same MDA as before. A more

significant benefit is enhancement of the signal-to-noise ratio (peak to continuum) for radon induced peaks (see insert in Fig. 7); this enables better monitoring of the background variation in shorter counting times (Hult et al., 2012).

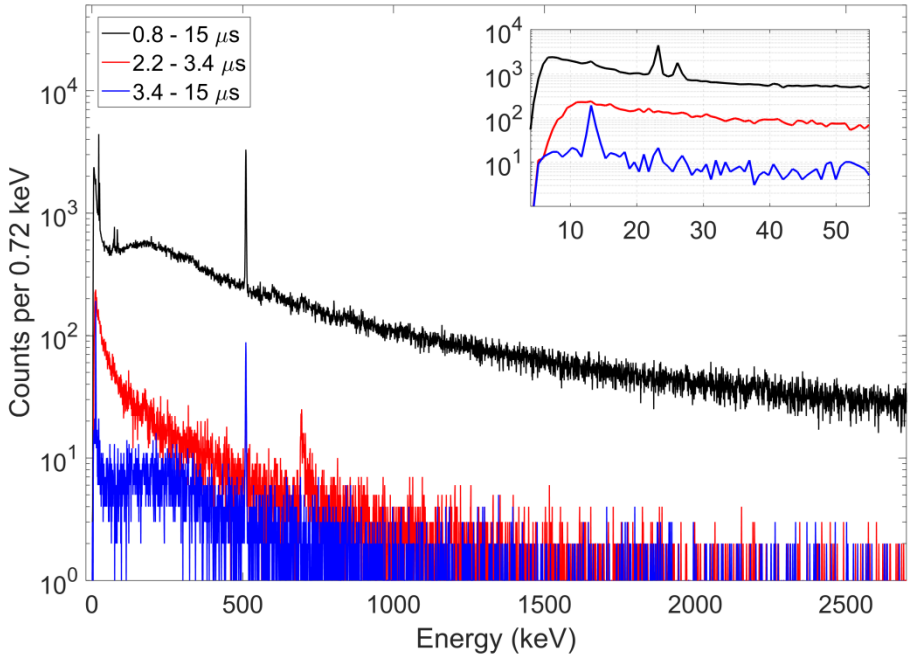

Fig. 6 HPGe spectra generated for three different coincidence delay ranges with a veto detector. The acquisition time was 15 days.

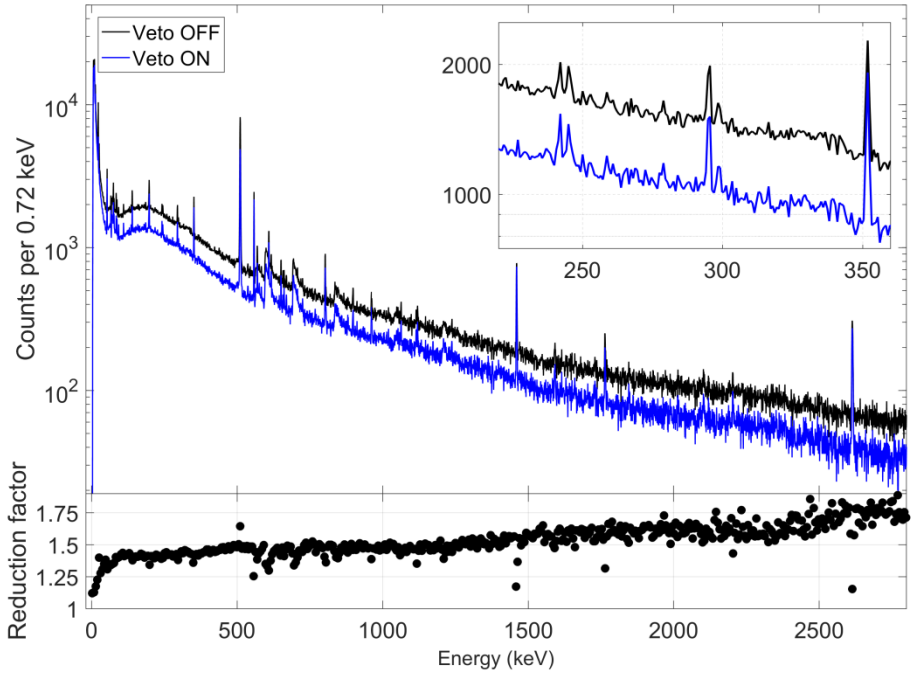

Fig.7 Background spectra from 15 days of measurement time. Anticoincidence width is 15 μs with an 0.8 μs delay. An energy threshold was applied to the veto pulses to remove the environmental gamma contribution. The bottom graph shows the energy dependence of the reduction factor.

The reduction factor for our system is almost the same as the one presented by (Hurtado et al., 2006), where a factor of 1.37 in 40-2715 keV range was reported; the authors used a single veto plate of a size similar to the one reported in this study (Hurtado et al., = 50x50x5 cm). A higher reduction factor of 4, using only a top plate (76x76 cm), is claimed by the LBNL group (Thomas et al., 2013). In addition to this, a reduction factor of 3 (50-2800 keV) was reported in (Mrđa et al., 2007), where authors used 5 plates to cover the detector from the top and four sides. An attempt was made to estimate the possible effect of using side plates, by calculating the solid angle covered by the veto plate convoluted with an angular flux distribution (muon flux ~$\cos^2\varphi$, where φ is zenith angle; (Particle Data Group, 1994). A ray-tracing simulation suggests that 61% of generated particles are stopped by the veto, meaning that the reduction factor with four additional plates would be around 2.4. The BEGe detector 'transparency' effect for muons was neglected here. The detector is thin and wide, so it was assumed that the side plate's contribution is higher because of the higher probability for interaction with muons hitting Ge crystal from the sides.

Table 3 provides a summary of peaks observed in the background gamma spectra. Three spectra are compared, analogue background spectrum, digital without anticoincidence and digital with the anticoincidence applied. This way the effect of digital acquisition peculiarities compared to analogue can be separated more clearly from the veto reduction effect. The integral count rate in the 40-2700 keV region was reduced by a factor of 1.4. The peak at 10.4 keV was assigned to K-shell EC line from ^{71}Ge thermal neutron activation (Aalseth et al., 2008) with 11.4 d half-life that explains why it was not suppressed by the veto. It is interesting to observe the difference in ^{73m}Ge lines in the digitally acquired spectrum and spectrum acquired using analogue system. In the latter, an analogue acquisition chain was used (2025 Canberra amplifier + 8701 ADC + 556 AIM) with a 6 μs amplifier shaping time. The first excited state of ^{73}Ge at 13.3 keV (already observed in Fig. 6) has a half-life of 2.92 μs, therefore the analogue system has a higher probability of summing 2->1 and 1->0 transitions in one 66.7 keV line (or pile-up somewhere between 53.4 and 66.7 keV). With the digital system, a trigger filter is able to discriminate the events when trapezoids (energy filters) overlap, but input rise-times are separated (CAEN Electronic Instrumentation, 2017); in our study trapezoid rise time was 4 μs and input rise time shifts to 0.95 μs. This is why the 53.4 keV line is not observed in the analogue system, while the sum peak at 66.7 keV is dominating. With the digital system the opposite applies. Another unexpected finding was the moderation effect of the plastic veto plate on neutron flux. Based on count rates in the 558.5 keV and 651.1 keV neutron induced lines in Cd (Fig. 2 and Table 3), it seems that the neutron spectrum is shifted towards lower energies. The cross section for the ^{113}Cd(n,γ)^{114}Cd reaction is a few orders of magnitude higher in the thermal than in the resonant region, when compared to thermal neutron induced reactions in Ge. Around a twofold increase in the total ^{73m}Ge count rate may also suggest an increase in thermal neutron flux, although the alternative explanation might be reduced pile-up in the digital system.

Because of the expected high neutron induced background and the changes in neutron flux with the plastic veto plate placed over the shield, in the following section estimates for the fast and thermal neutron flux are presented.

Table 3 Count rates in observed gamma lines with and without cosmic background reduction.

		Analog acquisition		Digital acquisition			
				Veto OFF		Veto ON	
E (keV)	Isotope /isomer	Count rate ($10^{-3}s^{-1}$)	Uncertainty ($10^{-3}s^{-1}$)	Count rate ($10^{-3}s^{-1}$)	Uncertainty ($10^{-3}s^{-1}$)	Count rate ($10^{-3}s^{-1}$)	Uncertainty ($10^{-3}s^{-1}$)
10.4	^{71m}Ge	6.42	0.19	6.34	0.16	6.29	0.15
13.2	^{73m}Ge	0.68	0.10	3.58	0.14	3.43	0.13

23.2	Cd Ka	5.37	0.13	5.73	0.11	2.37	0.09
26.1	Cd Kb	1.04	0.08	1.63	0.09	0.64	0.08
46.6	^{210}Pb	0.26	0.07	0.23	0.06	0.24	0.05
53.4	^{73m}Ge, ^{214}Pb	/	/	1.63	0.06	1.78	0.06
66.7	^{73m}Ge	1.58	0.08	0.52	0.05	0.55	0.06
110.0	^{235}U, ^{19}F	0.24	0.07	0.32	0.06	0.28	0.04
139.7	^{75m}Ge	0.85	0.06	0.88	0.05	0.92	0.05
185.9	^{235}U, ^{226}Ra	0.18	0.06	0.22	0.05	0.24	0.04
197.1	^{19}F[3]	0.42	0.07	0.50	0.06	0.44	0.05
198.3	^{71m}Ge	1.53	0.10	1.28	0.06	1.31	0.06
242	^{214}Pb	0.28	0.02	0.35	0.05	0.29	0.04
295.2	^{214}Pb	0.51	0.07	0.76	0.05	0.81	0.05
351.9	^{214}Pb	0.82	0.06	1.37	0.06	1.40	0.05
510.9	Annihilation	21.79	0.18	21.99	0.15	13.08	0.12
558.5	^{114*}Cd	1.99	0.06	2.86	0.06	2.74	0.06
569.7	^{207m}Pb	0.56	0.06	0.61	0.04	0.54	0.04
583.2	^{208}Tl	0.22	0.04	0.19	0.04	0.19	0.03
609.3	^{214}Bi	0.70	0.10	0.94	0.05	0.94	0.04
617.4	^{43*}Ca?	/	/	0.34	0.04	0.31	0.03
651.2	^{113}Cd(n,n)^{114}Cd	0.29	0.04	0.41	0.07	0.46	0.03
657.7	?	0.14	0.04	0.27	0.04	0.19	0.03
661.6	^{137}Cs	0.29	0.04	0.16	0.04	0.17	0.03
803	^{206*}Pb	0.94	0.05	0.86	0.04	0.88	0.03
1460.6	^{40}K	2.22	0.06	1.78	0.05	1.77	0.05
1764.5	^{214}Bi	0.35	0.03	0.33	0.03	0.40	0.03
2614.5	^{208}Tl	0.94	0.04	1.08	0.04	1.05	0.03
40-2700 keV		1310.0		1327.3		916.8	
40-2100 keV		1269.2		1272.9		883.3	
40-220 keV		367.2		367.8		264.3	
40-60 keV		42.0		43.7		32.5	

3.3 Cosmic-ray induced component and neutron flux

Neutrons ($T_{1/2}$ ~ 10 min), as well as muons ($T_{1/2}$ ~ 2 μs), are not part of primary cosmic rays. They are produced in showers originating in interactions of primary protons and alpha particles in the atmosphere. Galactic cosmic ray (GCR) particle fluxes display a latitudinal dependence (with more and lower energy particles penetrating the atmosphere close to the magnetic poles), modulated by 11 year solar cycles: this flux has an inverse relationship with solar activity as solar winds shield the Earth from GCR (Hathaway, 2010). Additional tertiary neutrons are produced by the interactions of protons and muons with high Z shielding material (Heusser, 1995). At zero overburden 92% of neutrons are produced by protons, and 8% by muons (Theodórsson, 1996). DTU Nutech laboratories are without any overburden so both secondary and tertiary neutrons are present. Proton flux attenuation by overburden thickness m, in meters of water equivalent (mwe), is proportional to $\sim e^{-\frac{m}{1.6\ \mathrm{mwe}}}$ (Theodórsson, 1996), while for the secondary neutrons it is $\sim e^{-\frac{m}{2\ \mathrm{mwe}}}$ (Gastrich et al.,

[3] Alternative is ^{77m}Ge 197.2 prompt gamma from ^{76}Ge(n,γ) reaction (Meierhofer et al., 2012).

2016). Consequently, already a shallow-depth of 5 mwe overburden reduces the neutron component by more than an order of magnitude.

There have been many attempts to connect the neutron flux and spectra with neutron induced lines in a gamma spectrum, e.g. (Fehrenbacher et al., 1996; Jovančević et al., 2010; Siiskonen and Toivonen, 2005), but when compared with accuracies of gamma spectrometric measurements it remains purely descriptive. That is unfortunate because low background gamma spectrometers have potential for use as sensitive neutron monitors (Chao and Chung, 1992).

The count rate in the neutron-induced peak is given by:

$$I = h(A)\omega(E)\varepsilon_{FEP}N_Z \int \sigma(E')\Phi(E')dE' \quad (1)$$

Where h(A) is isotopic abundance, N_Z number of atoms of element Z, ω(E) is transition probability, ε_{FEP} is the efficiency for detection of transition energy in full peak, σ(E') is a neutron cross section for creation of desired excited state, and Φ(E) neutron spectrum. As the neutron spectrum is not known and the cross sections are energy dependant, the problem can be solved only by modelling; e.g. unfolding of a priori neutron spectrum (Knežević et al., 2016). Here we will use experimentally derived estimate expressions for fast and slow neutron flux components (Škoro et al., 1992):

$$\Phi_F = k\frac{I(691.3\text{ keV})}{V} \quad (2)$$

for fast (E>691 keV neutron component). Where k=900±150, V is detector volume and I(691.3 keV) count rate in selected energy peak. For thermal neutron flux the expression is:

$$\Phi_T = 980\frac{I(139.7\text{ keV})}{V(\varepsilon_\gamma+1.6)} \quad (3)$$

Where εγ is FEP efficiency for 139.7 keV gamma ray generated inside the crystal.

Another approach is to rewrite Eq. (1) using average values for cross sections (Gastrich et al., 2016):

$$\Phi_T = \frac{I(139.7\ keV)}{\frac{\varepsilon_{FEP}(\gamma)+\alpha_T}{1+\alpha_T}N_{Ge}h(74)\sigma(n,\gamma)} \quad (4)$$

Where 100% efficiency for internal conversion electron absorption is assumed. For fast component:

$$\Phi_F = \frac{I(691.3\ keV)}{\varepsilon_{FEP}(e)N_{Ge}h(72)\sigma(n,\gamma)} \quad (5)$$

As de-excitation of the first excited state in ^{72}Ge is 100% through internal conversion (Jenkins et al., 2009). Efficiencies have been calculated using EGSnrc (Kawrakow et al., 2017) with an additional gamma spectrum generator (Lutter et al., 2017). ^{75m}Ge peak areas are calculated using Genie 2000 Interactive Peak Fit, while broad (saw-tooth) inelastic neutron scattering induced lines in ^{72}Ge are calculated using a fit to the convolution of the complementary error function (ERFC) and an exponential tail (Gete et al., 1997; Knežević et al., 2016; Siiskonen and Toivonen, 2005) in MATLAB. Table 4 presents the fast and thermal neutron fluxes with and without a veto plate on. The uncertainties are calculated according to GUM approach taking into account the peak area uncertainty obtained from fitting algorithm and full energy peak efficiency uncertainty of 15%. In comparison to the other reported values from surface laboratories (T:21 F:183 by (Wordel et al., 1996); T:64 F:510 by (Jovančević et al., 2010), T:179 F:510 by (Yoho et al., 2016)) our neutron flux appears to be similar, taking into account different geographical positions and shielding arrangements[4]. The flux reported by shallow laboratories, e.g. 10 mwe (Gastrich et al., 2016) are around two orders of magnitude lower.

Table 4 Neutron flux inside the lead shield calculated on the basis of count rates in the Ge activation lines ($m^{-2}s^{-1}$).

Reference	No plate	Plate	Veto
	Thermal flux $(\frac{n}{m^2 s})$		

[4] DTU Nutech gamma laboratory is at sea level.

	Φ	u(Φ)	Φ	u(Φ)	Φ	u(Φ)
Eq. (3), (Škoro et al., 1992)	22	2	23	1	24	1
Eq. (4), (Niese, 2008)(Gastrich et al., 2016)	21	1	22	1	22	1
	Fast flux ($\frac{n}{m^2 s}$)					
	Φ	u(Φ)	Φ	u(Φ)	Φ	u(Φ)
Eq. (2), (Škoro et al., 1992)	312	60	280	60	250	60
Eq. (5), (Niese, 2008)	370	70	340	70	300	60

4. Discussion and conclusions

Sources of background in a BEGe HPGe gamma spectrometer, in a surface laboratory have been identified and quantified. The laboratory does not have any overburden therefore cosmic ray induced background dominates. Application of muon component reduction with a cosmic veto resulted in total background reduction by a factor of 1.4. When translated into the gain in detection limits this gives MDA of 14 mBq for ^{60}Co for 2 days measurement time in 15 cm^3 petri dish, compared to 17 mBq without the veto reduction. The reduction factor of 1.4 is similar to published data on cosmic suppression by a single veto plate for surface laboratories. It has been estimated that surrounding the shield with four additional plates would yield a reduction factor of 2.4. Application of a dual input digital acquisition system in list-mode with time-stamped data for the HPGe detector and a cosmic veto enabled detailed investigation of parameter settings on the performance.
There are two important steps in veto optimization:

- Energy threshold selection for environmental gamma rejection.
- Coincidence timing selection to reject environmental pulses and cosmic pulses not interacting with HPGe detector.

Improper setting of the abovementioned parameters may lead to suboptimal efficiency of the veto system or high dead-time generation on other side. Generally, it is recommended to select wider coincidence window to reject as much as possible of the delayed emissions. This is especially important in underground/shallow laboratories where the count rates are lower, and veto has a bigger effect compared to surface laboratories (Theodórsson, 1996). In this study, we opted for a reasonably short coincidence window, based upon analysis that showed no relative benefits would be gained extending the window above 15 μs. A longer coincidence window would not introduce significant dead time but it would not reduce the background. Count rate in the muon part of our veto spectrum (total, not coincidence) was 37.5 cps; this agrees with 0.015 particles/cm^2 (Gilmore, 2008); even without the coincidence criteria the direct gate would only introduce <0.5% dead time. The energy threshold is a sensitive parameter because it can introduce significant dead time if not set properly. If the system is sensitive to environmental gamma background the dead time can change, e.g. with movement of the sources in the laboratory. Therefore, if the veto is not shielded the environmental component should be cut-off. The veto detector should be set with short amplifying constants and high LLD (noise cut-off) to avoid dead time in veto.
The thermal and fast neutron fluxes were calculated from the peak areas of the gamma lines originating from neutron capture and inelastic scattering reactions in germanium crystal.
In addition to the cosmic component investigation, the radon and daughters' background was measured over a long period. The big oscillations observed called for immediate action, so a flushing step with nitrogen from the Dewar was introduced and a detector cover fitted to decrease the air exchange in the shield. This resulted in satisfactory radon (variation) levels.

Unfortunately, the lack of overburden remains the main problem so further investment in background reduction is assessed as being unjustified.

References

Aalseth, C.E., Barbeau, P.S., Cerdeño, D.G., Colaresi, J., Collar, J.I., De Lurgio, P., Drake, G., Fast, J.E., Greenberg, C.H., Hossbach, T.W., Kephart, J.D., Marino, M.G., Miley, H.S., Orrell, J.L., Reyna, D., Robertson, R.G.H., Talaga, R.L., Tench, O., Van Wechel, T.D., Wilkerson, J.F., Yocum, K.M., 2008. Experimental constraints on a dark matter origin for the DAMA annual modulation effect. Phys. Rev. Lett. 101, 1–4.

Abriola, D., Sonzogni, A.A., 2010. Nuclear Data Sheets for A = 72*. Nucl. Data Sheets 111, 1–140.

Agostini, M., Allardt, M., Andreotti, E., Bakalyarov, A.M., Balata, M., Barabanov, I., Barnabe, M., Barros, N., Baudis, L., Bauer, C., Bellotti, E., Belogurov, S., Belyaev, S.T., Caldwell, A., Benato, G., Bettini, A., Bezrukov, L., Bode, T., Brudanin, V., Brugnera, R., Budja, D., Cattadori, C., Chernogorov, A., Cossavella, F., Demidova, E. V, Domula, A., Egorov, V., Falkenstein, R., Ferella, A., Freund, K., Frodyma, N., Gangapshev, A., Garfagnini, A., Gotti, C., Grabmayr, P., Gurentsov, V., Gusev, K., Guthikonda, K.K., Hampel, W., Hegai, A., Heisel, M., Hemmer, S., Jochum, J., Heusser, G., Hofmann, W., Hult, M., Inzhechik, L. V, Ioannucci, L., Janicsko, J., Kochetov, O., Junker, M., Kihm, T., Kirpichnikov, I. V, Kirsch, A., Klimenko, A., Kno, K.T., Kornoukhov, V.N., Kuzminov, V. V, Laubenstein, M., Lazzaro, A., Lebedev, V.I., Lehnert, B., Liao, H.Y., Lindner, M., Lippi, I., Liu, X., Lubashevskiy, A., Lubsandorzhiev, B., Lutter, G., Macolino, C., Machado, A.A., Majorovits, B., Maneschg, W., Misiaszek, M., Nemchenok, I., Nisi, S., Pandola, L., Pelczar, K., Pessina, G., Pullia, A., Riboldi, S., Rumyantseva, N., Sada, C., Salathe, M., Schmitt, C., Shevchik, E., Shirchenko, M., Simgen, H., Schreiner, J., Schulz, O., Schwingenheuer, B., Scho, S., Smolnikov, A., Stanco, L., Strecker, H., Tarka, M., Ur, C.A., Vasenko, A.A., Volynets, O., Wagner, V., Walter, M., Wegmann, A., Wester, T., Wojcik, M., Yanovich, E., Zavarise, P., Zhitnikov, I., Zhukov, S. V, Zinatulina, D., Zuber, K., Zuzel, G., 2013. Results on Neutrinoless Double-β Decay of 76Ge from Phase I of the GERDA Experiment. Phys. Rev. Lett. 111, 1–6.

Agostini, M., Barnabé-Heider, M., Budjáš, D., Cattadori, C., Gangapshev, A., Gusev, K., Heisel, M., 2015. LArGe: active background suppression using argon scintillation for the Gerda 0νββ-experiment. Eur. Phys. J. C 75.

Bruggeman, M., Verheyen, L., Vidmar, T., 2014. A dedicated LIMS for routine gamma-ray spectrometry. Appl. Radiat. Isot. 87, 425–428.

Burnett, J.L., Davies, A. V, 2014. Cosmic veto gamma-spectrometry for Comprehensive Nuclear-Test-Ban Treaty samples. Nucl. Inst. Methods Phys. Res. A 747, 37–40.

C. Patrignani et al. (Particle Data Group), 2016. Review of Particle Physics. Chinese Phys. C 40, 100001.

CAEN Electronic Instrumentation, 2017. MC2Analyzer User Manual Software for digital Multi Channel Analyzer, User Manual UM3182.

Canberra, 2013. Genie^{TM} 2000 Spectroscopy Software Customization Tools Manual.

Canberra, 2009. Model S506 Interactive Peak Fit User's Manual.

Chao, J., Chung, C., 1992. Low-level neutron monitoring by use of germanium detectors. Nucl. Inst. Methods Phys. Res. A 321, 535–538.

Currie, L.A., 1968. Limits for Qualitative Detection and Quantitative Determination Application to Radiochemistry. Anal. Chem. 40, 586–593.

Dragounová, L., Rulík, P., 2013. Low level activity determination by means of gamma spectrometry with respect to the natural background fluctuation. Appl. Radiat. Isot. 81, 123–127.

Fehrenbacher, G., Meckbach, R., Paretzke, H.G., 1996. Fast neutron detection with germanium detectors: Computation of response functions for the 692 keV inelastic scattering peak. Nucl. Instruments Methods Phys. Res. Sect. A Accel. Spectrometers, Detect. Assoc. Equip. 372, 239–245.

Gastrich, H., Gößling, C., Klingenberg, R., Kröninger, K., Neddermann, T., Nitsch, C., Quante, T., Zuber, K., 2016. The Dortmund Low Background Facility — Low-background gamma ray spectrometry with an artificial overburden. Appl. Radiat. Isot. 112, 165–176.

Gete, E., Measday, D.F., Moftah, B.A., Saliba, M.A., Stocki, T.J., 1997. Neutron-induced peaks in Ge detectors from evaporation neutrons. Nucl. Inst. Methods Phys. Res. A 388, 212–219.

Gilmore, G.R., 2008. Practical Gamma-ray Spectrometry, 2nd ed. Wiley.

Hathaway, D.H., 2010. The solar cycle. Living Rev. Sol. Phys. 7.

Heusser, G., 1995. Low-Radioactivity Background Techniques. Ann. Rev. Nucl. Part. Sci. 45, 543–90.

Heusser, G., 1991. Studies of y-ray background with a low level germanium spectrometer. Nucl. Inst. Methods Phys. Res. B 58, 79–84.

Heusser, G., Weber, M., Hakenmüller, J., Laubenstein, M., Lindner, M., Maneschg, W., Simgen, H., Stolzenburg, D., Strecker, H., 2015. GIOVE: a new detector setup for high sensitivity germanium spectroscopy at shallow depth. Eur. Phys. J. C 75, 1–16.

Hult, M., 2007. Low-level gamma-ray spectrometry using Ge-detectors. Metrologia 44, S87–S94.

Hult, M., Andreotti, E., De Orduña, R.G., Pommé, S., Yeltepe, E., 2012. Quantification of uranium-238 in environmental samples using gamma-ray spectrometry. EPJ Web Conf. 24, 1–12.

Hult, M., Lutter, G., Yüksel, A., Marissens, G., Misiaszek, M., 2013. Comparison of background in underground HPGe-detectors in different lead shield con fi gurations. Appl. Radiat. Isot. 81, 103–108.

Hurtado, S., Garcia-Leon, M., Garcia-Tenorio, R., 2006. Optimized background reduction in low-level gamma-ray spectrometry at a surface laboratory. Appl. Radiat. Isot. 64, 1006–1012.

IAEA, 2017. Determination and Interpretation of Characteristic Limits for Radioactivity Measurements.

ISO, 2019. ISO 11929:2019 Determination of the characteristic limits (decision threshold, detection limit and limits of the coverage interval) for measurements of ionizing radiation.

Jenkins, D.G., Glover, R., Herzberg, R.D., Boston, A.J., Gray-Jones, C., Nordlund, A., 2009. Proof-of-principle for fast neutron detection with advanced tracking arrays of highly segmented germanium detectors. Nucl. Instruments Methods Phys. Res. Sect. A Accel. Spectrometers, Detect. Assoc. Equip. 602, 457–460.

Jovančević, N., Krmar, M., Mrda, D., Slivka, J., Bikit, I., 2010. Neutron induced background gamma activity in low-level Ge-spectroscopy systems. Nucl. Inst. Methods Phys. Res. A 612, 303–308.

Kawrakow, I., Mainegra-Hing, E., Rogers, D.W.O., Tessier, F., Walters, B.R.B., 2017. The EGSnrc Code System: Monte Carlo Simulation of Electron and Photon Transport. Ottawa, Canda.

Knežević, D., Jovančević, N., Krmar, M., Petrović, J., 2016. Modeling of neutron spectrum in the gamma spectroscopy measurements with Ge-detectors. Nucl. Instruments Methods Phys. Res. Sect. A Accel. Spectrometers, Detect. Assoc. Equip. 833, 23–26.

Korun, M., Vodenik, B., Zorko, B., 2014. Determination of the shielding factors for gamma-ray spectrometers. Appl. Radiat. Isot. 87, 372–375.

Leo, W.R., 1994. Techniques for Nuclear and Particle Physics Experiments, 2nd ed. Springer-Verlag.

Lépy, M.C., Pearce, A., Sima, O., 2015. Uncertainties in gamma-ray spectrometry. Metrologia 52, S123–S145.

Lutter, G., Hult, M., Tzika, F., Stroh, H., Marissen, G., 2017. Gamma-ray spectrometry analysis software environment. Appl. Radiat. Isot.

Marković, N., Roos, P., Hou, X., Lutter, G., Nielsen, S.P., 2018. Calibration of HPGe – HPGe coincidence spectrometer through performing standardisation of 125I activity by X-ray-gamma coincidence spectrometry using two HPGe detectors. Nucl. Inst. Methods Phys. Res. A 880, 194–200.

Marković, N., Roos, P., Nielsen, S.P., 2017a. Digital gamma-gamma coincidence HPGe system for environmental analysis. Appl. Radiat. Isot. 126, 194–196.

Marković, N., Roos, P., Nielsen, S.P., 2017b. Low-level gamma-ray spectrometry for the determination of 210Pb. J. Radioanal. Nucl. Chem. 311, 1473–1478.

Mauring, A., Gäfvert, T., Bandur Aleksandersen, T., 2014. Implications for analysis of 226Ra in a low-level gamma spectrometry laboratory due to variations in radon background levels. Appl. Radiat. Isot. 94, 54–59.

Maver Modec, P., Korun, M., Martelanc, M., Vodenik, B., 2012. A comparative study of the radon-induced background in low-level gamma-ray spectrometers. Appl. Radiat. Isot. 70, 324–331.

Meierhofer, G., Grabmayr, P., Canella, L., Kudejova, P., Jolie, J., Warr, N., 2012. Prompt γ rays in 77Ge and 75Ge after thermal neutron capture. Eur. Phys. J. A 48, 20.

Mrđa, D., Bikit, I., Zikić-Todorović, N., S., F., Slivka, J., Vesković, M., 2007. First tests of the active shield for a gamma ray spectrometer. Radiat. Meas. 42, 1361–1367.

Niese, S., 2008. Underground laboratories for low-level radioactivity measurements, in: Povinec, P.P. (Ed.), Analysis of Environmental Radionuclides. Elsevier, pp. 209–239.

Particle Data Group, 1994. Review of particle properties. Phys. Rev. D 50, 1269.

Pommé, S., Stroh, H., Paepen, J., Van Ammel, R., Marouli, M., Altzitzoglou, T., Hult, M., Kossert, K., Nähle, O., Schrader, H., Juget, F., Bailat, C., Nedjadi, Y., Bochud, F., Buchillier, T., Michotte, C., Courte, S., van Rooy, M.W., van Staden, M.J., Lubbe, J., Simpson, B.R.S., Fazio, A., De Felice, P., Jackson, T.W., Van Wyngaardt, W.M., Reinhard, M.I., Golya, J., Bourke, S., Roy, T., Galea, R., Keightley, J.D., Ferreira, K.M., Collins, S.M., Ceccatelli, A., Unterweger, M., Fitzgerald, R., Bergeron, D.E., Pibida, L., Verheyen, L., Bruggeman, M., Vodenik, B., Korun, M., Chisté, V., Amiot, M.N., 2016. Evidence against solar influence on nuclear decay constants. Phys. Lett. Sect. B Nucl. Elem. Part. High-Energy Phys. 761, 281–286.

Rios, R., Tatar, E., Bacon, J.D., Bowles, T.J., Hill, R., Green, J.A., Hogan, G.E., Ito, T.M., Makela, M., Morris, C.L., Mortenson, R., Pasukanics, F.E., Ramsey, J., Saunders, A., Seestrom, S.J., Sondheim, W.E., Teasdale, W., Saltus, M., Back, H.O., Cottrell, C.R., Holley, A.T., Pattie, R.W., Young, A.R., Broussard, L.J., Filippone, B.W., Hickerson, K.P., Liu, J., Mendenhall, M.P., Plaster, B., Mammei, R.R., Pitt, M.L., Vogelaar, R.B., Martin, J.W., 2011. Sealed drift tube cosmic ray veto counters. Nucl. Instruments Methods Phys. Res. Sect. A Accel. Spectrometers, Detect. Assoc. Equip. 637, 105–108.

Siiskonen, T., Toivonen, H., 2005. A model for fitting peaks induced by fast neutrons in an HPGe detector. Nucl. Instruments Methods Phys. Res. Sect. A Accel. Spectrometers, Detect. Assoc. Equip. 540, 403–411.

Singh, B., 2004. Nuclear Data Sheets for A = 73 *. Nucl. Data Sheets 101, 193–323.

Škoro, G.P., Aničin, I.V., Kukoč, A.H., Krmpotić, D., Adžić, P., Vukanović, R., Župančić, M., 1992. Environmental neutrons as seen by a germanium gamma-ray spectrometer. Nucl. Inst. Methods Phys. Res. A 316, 333–336.

Theodórsson, P., 1996. Measurement of Weak Radioactivity. World Scientific.

Thomas, K.J., Norman, E.B., Smith, A.R., Chan, Y.D., 2013. Installation of a muon veto for low background gamma spectroscopy at the LBNL low-background facility. Nucl. Inst. Methods Phys. Res. A 724, 47–53.

Turunen, J., Ihantola, S., Peräjärvi, K., Pöllänen, R., Toivonen, H., Hrnecek, E., 2011. Collection and behaviour of radon progenies on thin Mylar foils. Radiat. Meas. 46, 631–634.

Verplancke, J., 1992. Low level gamma spectroscopy: low, lower, lowest. Nucl. Inst. Methods Phys. Res. A 312, 174–182.

Wieslander, J.S.E., Hult, M., Gasparro, J., Marissens, G., Misiaszek, M., Preusse, W., 2009. The Sandwich spectrometer for ultra low-level γ-ray spectrometry. Appl. Radiat. Isot. 67, 731–735.

Wordel, R., Mouchel, D., Altzitzoglou, T., Heusser, G., Arnes, B.Q., P.Meynendonckx, 1996. Study of neutron and muon background in low-level germanium gamma-ray spectrometry. Nucl. Inst. Methods Phys. Res. A 369, 557–562.

Yoho, M., Porterfield, D.R., Landsberger, S., 2016. Quality assurance of temporal variability of natural decay chain and neutron induced background for low-level NORM analysis. J. Radioanal. Nucl. Chem. 307, 2459–2463.

Zhang, W., Ro, H., Liu, C., Hoffman, I., Ungar, K., 2017. Design and Optimization of a Dual-HPGe Gamma Spectrometer and Its Cosmic Veto System. IEEE Trans. Nucl. Sci. 64, 894–900.

Captions

Fig. 1 Schematic representation of a BEGe detector inside a lead shield with a plastic veto plate placed on top (dimensions in mm). The shield opens by sliding the lid.

Fig. 2 Variation in background count rate of natural sources, radon daughters and ^{40}K, is shown in a). In September 2017, flushing with the boil-off gas from the nitrogen dewar was initiated, reducing the overall Rn background and its variability (indicated with vertical line). Variation in peak count rates of cosmic induced lines and integral background are shown in b) and c).

Fig. 3 Total spectrum count rate in the 40-2100 keV interval as a function of the sum of count rates in three radon daughter peaks (295 keV, 352 keV and 609 keV).

Fig. 4 Time distribution of differences in signal generation between the coincident events in the HPGe, and the veto detector (time when an event is registered in the HPGe, minus the time stamp of the closest veto event). If environmental background counts are not discriminated in the veto detector, then random coincidence continuum is high (black curve). By setting the LLD to around 5 MeV on the veto detector, the random coincidence count rate is reduced, and timing properties become clearer.

Fig. 5 Cosmic veto detector spectra generated over a 5 day interval. Spectrum of coincidences for the HPGE detector (15 μs width and 0.8 μs delay) is shown in blue. The peak centred around 10 MeV originates from muons passing through the plate. For the low energy range (up to 3 MeV), the source is environmental background radiation. Threshold energy for separation of environmental background and muon events is set in the middle of plateau between the two peaks, at around 5 MeV. It is used in conjunction with time coincidence to reduce random coincidences between the environmental background in the veto detector and counts in the HPGe detector.

Fig. 6 HPGe spectra generated for three different coincidence delay ranges with a veto detector. The acquisition time was 15 days.

Fig.7 Background spectra from 15 days of measurement time. Anticoincidence width is 15 μs with an 0.8 μs delay. An energy threshold was applied to the veto pulses to remove the environmental gamma contribution. The bottom graph shows the energy dependence of the reduction factor.

Table 1 Variation in background count rates before and after Rn reduction. Rn average values are reduced by a factor of 2-3 and variability up to an order of magnitude.

Table 2 Background variation effect on activity calculation for two standard beakers (before the radon component remediation was installed).

Table 3 Count rates in observed gamma lines with and without cosmic background reduction.

Table 4 Neutron flux inside the lead shield calculated on the basis of count rates in the Ge activation lines ($m^{-2}s^{-1}$).